Supplementary Information on

Mesoscopic analyses of the morphology and operation conditions on the transport resistances in a proton-exchange-membrane fuel-cell catalyst layer

Yu-Tong Mu, Adam Z. Weber, Zhao-Lin Gu, Tobias Schuler, Wen-Quan Tao

1. Electrochemical reaction rate

The electrochemical reaction rate j (A·m^{-2}) is calculated as [1]

$$j = j_0 \left(\frac{c_{\mathrm{O_2,Pt}}}{c_{\mathrm{O_2,ref}}} \right)^{\gamma_c} (1-\theta) \exp\left(\frac{-\alpha_c F \eta_c}{RT} \right) \exp\left(\frac{-\omega_c \theta}{RT} \right) \tag{S1}$$

$$j_0 = j_0^{\mathrm{ref}} \exp\left(-\frac{E_c}{R} \left(\frac{1}{T} - \frac{1}{353.15} \right) \right) \tag{S2}$$

where α_c, β_c, γ_c and η_c are the transfer coefficient, the energy parameter for the Temkin isotherm, the oxygen reaction order, and the cathode overpotential, respectively. The oxide coverage θ is a function of the cathode potential Φ (cell voltage) relative to hydrogen reference electrode [2],

$$\theta = 1 \Big/ \left[1 + \exp\left(22.4 \left(0.818 - \Phi \right) \right) \right] \tag{S3}$$

with Φ approximately calculated as,

$$\Phi = E + \eta_c - \eta_a - i l_m / \kappa_m \tag{S4}$$

where i, l_m, κ_m, and η_a denote to the current density, the membrane thickness, the proton conductivity, and the anode overpotential. η_a can be neglected due to a fast hydrogen oxidation reaction rate. η_c is treated as an input parameter, which is uniformly distributed throughout the cathode CL. The reversible voltage E is determined by E=1.229-0.846×10^{-3}(T-298.15), and κ_m is calculated as [3]

$$\kappa_m = (0.5139\lambda - 0.326) \exp\left[1268 \left(\frac{1}{303} - \frac{1}{T} \right) \right] \tag{S5}$$

2. Multiple-relaxation-time lattice Boltzmann method

The MRT collision operator is used due to its higher numerical stability achieved by adjusting the separated relaxation times representing changes in different physical processes

[4]. In the present study, the D3Q7 (7 discrete velocities in 3 dimensions) model is selected for its simplicity. The evolutions of the distribution functions are expressed as

$$\hat{f}_\alpha(\mathbf{x},t)=f_\alpha(\mathbf{x},t)+\sum_{\beta=0}^{6}L_{\alpha\beta}\left(f_\beta(\mathbf{x},t)-f_\beta^{\mathrm{eq}}(\mathbf{x},t)\right)\text{ and }f_\alpha(\mathbf{x}+\mathbf{e}_\alpha\delta t,t+\delta t)=\hat{f}_\alpha(\mathbf{x},t) \quad \text{(S6a)}$$

$$\hat{g}_\alpha(\mathbf{x},t)=g_\alpha(\mathbf{x},t)+\sum_{\beta=0}^{6}L_{\alpha\beta}\left(g_\beta(\mathbf{x},t)-g_\beta^{\mathrm{eq}}(\mathbf{x},t)\right)\text{ and }g_\alpha(\mathbf{x}+\mathbf{e}_\alpha\delta t,t+\delta t)=\hat{g}_\alpha(\mathbf{x},t) \quad \text{(S6b)}$$

where $f_\alpha(\mathbf{x}, t)$ and $g_\alpha(\mathbf{x}, t)$ denote to the distribution function at the lattice site $\mathbf{x}$ and time t in the αth direction for oxygen and vapor. $\hat{\mathbf{f}}$ and $\hat{\mathbf{g}}$ denote to the post-collision populations of oxygen and vapor, respectively. The lattice velocity $\mathbf{e}_\alpha$ and the weight coefficient ω_α are given as: $\mathbf{e}_0$=[0, 0, 0], $\mathbf{e}_1$=[c, 0, 0], $\mathbf{e}_2$=[$-c$, 0, 0], $\mathbf{e}_3$=[0, c, 0], $\mathbf{e}_4$=[0, $-c$, 0], $\mathbf{e}_5$=[0, 0, c] , $\mathbf{e}_6$=[0, 0, $-c$], and $\omega_{0\text{-}6}$=1/7 with the lattice sound speed $c=\delta x/\delta t$. Since the convective effect is neglected, the respective equilibrium distribution functions $f_\beta^{\mathrm{eq}}(\mathbf{x},t)$ and $g_\beta^{\mathrm{eq}}(\mathbf{x},t)$ are given as $f_\beta^{\mathrm{eq}}(\mathbf{x},t)=\omega_\beta\phi_{\mathrm{O_2}}$ and $g_\beta^{\mathrm{eq}}(\mathbf{x},t)=\omega_\beta\phi_{\mathrm{H_2O}}$ with the macroscopic concentrations of oxygen and vapor calculated as $\phi_{\mathrm{O_2}}=\sum_{\alpha=0}^{6}f_\alpha(\mathbf{x},t)$ and $\phi_{\mathrm{H_2O}}=\sum_{\alpha=0}^{6}g_\alpha(\mathbf{x},t)$. Specifically, ϕ_{O2} can represent the oxygen concentration at pores, ionomer and liquid water if the nodes correspond to the above components. ϕ_{H2O} can represent the water concentration at pores and ionomer. To distinguish different components for the transport processes, the relaxation coefficients related with the diffusion coefficients are given as,

$$\tau_{ij}=\frac{1}{2}\delta_{ij}+\frac{7D_{ij}}{2c\delta x} \quad \text{(S7)}$$

As isotropic diffusion is considered, the following relationship of the relaxation coefficients are applied,

$$\tau_{00}=1,\ \tau_{44}=\tau_{55}=\tau_{66}=\frac{1}{2}+\frac{1}{6\left(\tau_{11,22,33}-1/2\right)} \quad \text{(S8)}$$

The relaxation coefficient τ_{11}=τ_{22}=τ_{33} can be chosen as high as 10000. Its robustness on the numerical method has been validated in our previous study [5]. The MRT collision operator $\mathbf{L}$ can be described as $\mathbf{L}=\mathbf{M}^{-1}\mathbf{\Lambda}\mathbf{M}$ with the transformation matrix $\mathbf{M}$ and its corresponding diagonal matrix $\mathbf{\Lambda}$ provided as follows:

$$\mathbf{M}=\begin{pmatrix}1&1&1&1&1&1&1\\0&1&-1&0&0&0&0\\0&0&0&1&-1&0&0\\0&0&0&0&0&1&-1\\6&-1&-1&-1&-1&-1&-1\\0&2&2&-1&-1&-1&-1\\0&0&0&1&1&-1&-1\end{pmatrix} \text{ and } \mathbf{\Lambda}^{-1}=\begin{pmatrix}\tau_{00}&0&0&0&0&0&0\\0&\tau_{11}&0&0&0&0&0\\0&0&\tau_{22}&0&0&0&0\\0&0&0&\tau_{33}&0&0&0\\0&0&0&0&\tau_{44}&0&0\\0&0&0&0&0&\tau_{55}&0\\0&0&0&0&0&0&\tau_{66}\end{pmatrix} \tag{S9}$$

3. Conjugated interfacial condition treatments

To deal with the conjugated boundary conditions described in Eqs. (8), (16), (18) and (20), special attention needs to be paid to the numerical treatments. As depicted in Fig. S1, the respective unknown populations for the oxygen transport at $\mathbf{x_A}$ and $\mathbf{x_B}$ are f_4 ($\mathbf{x_A}$, t+δt) and f_3 ($\mathbf{x_B}$, t+δt). The rest of the populations are known. Detailed analyses of the numerical treatments are given as follows:

(1) Letting $\mathbf{x}_\mathrm{A}$ represent pores and $\mathbf{x}_\mathrm{B}$ represent ionomer or liquid water, numerical treatments on the unknown populations of oxygen at the interfaces are specified as [5]

$$f_4\left(\mathbf{x}_\mathrm{A},t+\delta t\right)=\frac{\left(\varepsilon_\mathrm{D}c/k_\mathrm{dis}+1/K-1\right)\hat{f}_3\left(\mathbf{x}_\mathrm{A},t\right)-2\hat{f}_4\left(\mathbf{x}_\mathrm{B},t\right)}{\varepsilon_\mathrm{D}c/k_\mathrm{dis}-1/K-1} \tag{S10a}$$

$$f_3\left(\mathbf{x}_\mathrm{B},t+\delta t\right)=\frac{\left(\varepsilon_\mathrm{D}c/k_\mathrm{dis}-1/K+1\right)\hat{f}_4\left(\mathbf{x}_\mathrm{B},t\right)-2/K\,\hat{f}_3\left(\mathbf{x}_\mathrm{A},t\right)}{\varepsilon_\mathrm{D}c/k_\mathrm{dis}-1/K-1} \tag{S10b}$$

where the parameter ε_D equals 2/7. The partition coefficient K equals H/RT for the ionomer nodes or H_liq/RT for the liquid water. For the vapor transport at the interfaces, Eq. (S10) can be simplified as $g_4\left(\mathbf{x}_\mathrm{A},t+\delta t\right)=\hat{g}_4\left(\mathbf{x}_\mathrm{B},t\right)$ and $g_3\left(\mathbf{x}_\mathrm{B},t+\delta t\right)=\hat{g}_3\left(\mathbf{x}_\mathrm{A},t\right)$.

(2) Let $\mathbf{x}_\mathrm{A}$ represent ionomer and $\mathbf{x}_\mathrm{B}$ represent Pt particles, numerical treatments on the populations of oxygen at the interfaces can be solved with a set of equations below by using Newton-Raphson iterative method as γ_c in Eq. (S1) is chosen as 0.8,

$$f_4\left(\mathbf{x}_\mathrm{A},t+\delta t\right)=\varepsilon_\mathrm{D}c_{\mathrm{O_2,\,ion}}-\hat{f}_3\left(\mathbf{x}_\mathrm{A},t\right) \tag{S11a}$$

$$\hat{f}_3\left(\mathbf{x}_\mathrm{A},t\right)-f_4\left(\mathbf{x}_\mathrm{A},t+\delta t\right)=k_\mathrm{ads}\frac{\delta t}{\delta x}\left(c_{\mathrm{O_2,\,ion}}-c_{\mathrm{O_2,\,Pt}}\right)=\frac{\delta t}{\delta x}\frac{j}{4F} \tag{S11b}$$

$$g_4\left(\mathbf{x}_\mathrm{A},t+\delta t\right)=\varepsilon_\mathrm{D}c_{\mathrm{H_2O,\,ion}}-\hat{g}_3\left(\mathbf{x}_\mathrm{A},t\right) \tag{S11c}$$

$$g_4\left(\mathbf{x}_\mathrm{A},t+\delta t\right)-\hat{g}_3\left(\mathbf{x}_\mathrm{A},t\right)=\frac{\delta t}{\delta x}S_{\mathrm{H_2O}} \tag{S11d}$$

where $c_{O2,ion}$ and $c_{O2,Pt}$ are the unknown oxygen concentration at the interfaces of Pt/ionomer. $c_{H2O,ion}$ is the unknown vapor concentration at the Pt/ionomer interfaces. Combined with Eqs. (S1) and (20), the unknown populations f_4 and g_4 can be obtained. For a comprehensive detailed derivation processes, readers can refer to our previous work [5, 6].

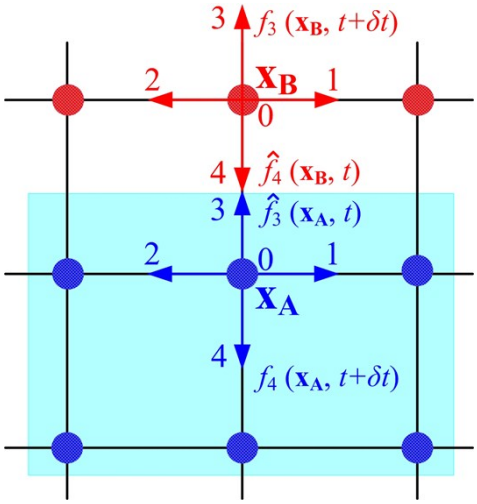

Fig. S1 Numerical treatments of the conjugated mass-transport process in the CL

4. Simulation flowchart of the model

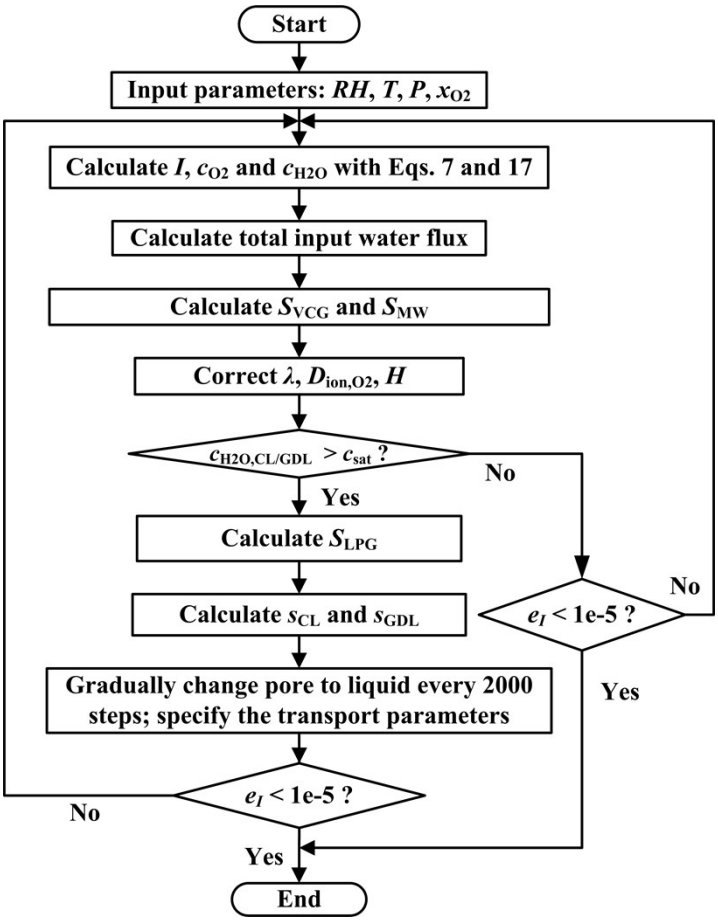

Fig. S2 Simulation flowchart

5. Thickness-dependent distributions of several transport parameters in CL

The surface-average physical quantity, defined as the sum of which its corresponding nodes normalized by its total nodes at a given cross-section, is presented in Fig. S3 (a). As seen, $c_{p,O2}$ decreases slightly along the thickness, with its value at x=0 decreasing with L_{Pt} as demonstrated before. Higher $c_{p,O2}$ drop is expected for higher L_{Pt} as i_{lim} increases. Fig. S3 (b) illustrates the oxygen concentration contour for the thickness ranging from 5.5 to 6.5 μm. Little difference can be observed, indicating the oxygen concentration in pores is relatively uniform. On the contrary, the oxygen in ionomer $c_{Ion,O2}$ differs greatly due to the following two reasons. First is the unevenness of the ionomer thickness coated on the carbon particles, resulting in different local transport resistance for the oxygen transporting from pores to ionomer; the second is the different electrochemical reaction rate j, which is highly related with $c_{Ion,O2}$ and the Pt particles distribution on Pt/C mixtures. Large oscillation of $c_{Ion,O2}$ can be observed in Fig. S3 (b). $c_{Ion,O2}$ is in the order of 10^{-2} mol□m^{-3}, which is about one magnitude-order lower than $c_{p,O2}$ due to a small dissolved solubility of oxygen in ionomer and the electrochemical reaction at the Pt/ionomer surfaces. Compared with the distributions of oxygen concentrations, the vapor concentrations in pores $c_{p,H2O}$ increases along the thickness direction due to the water production. Liquid water does not exist as the local $c_{p,H2O}$ is below the saturated concentration. $c_{p,H2O}$ increases with L_{Pt} as higher current density is produced. Correspondingly, the water content λ in the ionomer increases along the thickness direction slightly. As the bulk transport resistance R_I caused by the ionomer thin-film decreases with λ, it is expected that the contribution of the bulk resistance R_I to the total local transport resistance $R_{O_2}^{Pt}$ may be less significant with L_{Pt}. Fig. S3 (c) illustrates the water concentration contour and the surface reaction rate j for the thickness ranging from 5.5 to 6.5 μm. At the Pt/ionomer interfaces, j presents a similar trend with $c_{Pt,O2}$. Despite of the relatively lower j for higher L_{Pt}, the total current density is much higher (see Fig. 3) as f_{Pt} increases with L_{Pt}. This also confirms the fact that the flux per platinum site increases with decreasing loading.

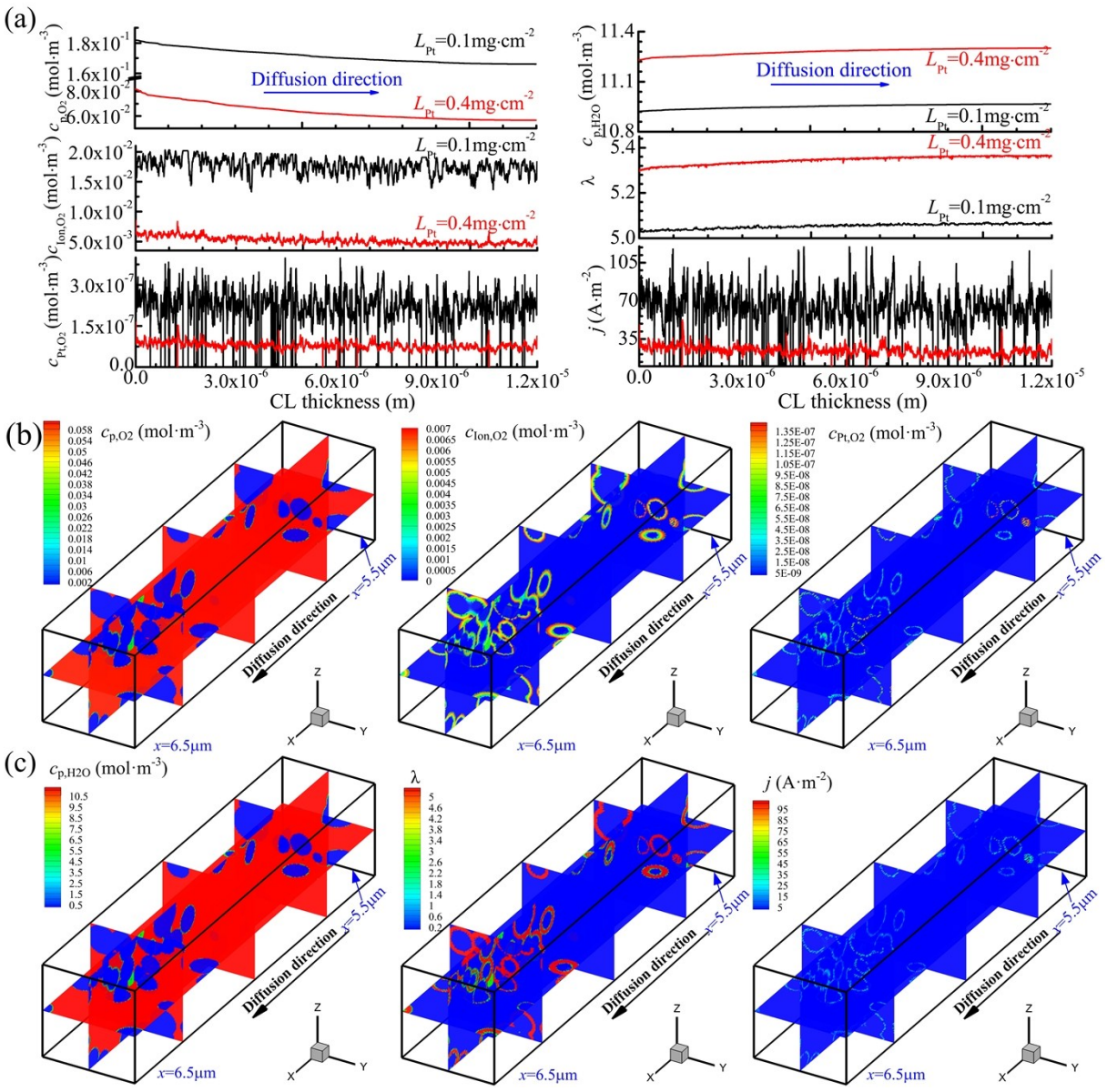

Fig. S3 Thickness-dependent distributions of several critical transport parameters at i_{lim}, (a) oxygen concentrations in pores $c_{p,O2}$, ionomer thin-films $c_{Ion,O2}$, Pt surfaces $c_{Pt,O2}$, vapor concentration in pores $c_{p,H2O}$, water content in ionomer thin-films λ, and the surface reaction rate j; (b) contours of oxygen concentrations in pores $c_{p,O2}$, ionomer thin-films $c_{Ion,O2,}$ and Pt surfaces $c_{Pt,O2,}$ for case 3; (c) contours of water concentrations in pores $c_{p,H2O}$, ionomer thin-films $c_{Ion,H2O,}$ and the surface reaction rate j for case 3

6. Validation of the assumptions of the electronic and ionic isopotentials

To examine the reliability of this assumption, a 1-D cathode CL simulation is performed. Fig. S4 presents an illustration of 1-D cathode CL model. The governing equations are given as follows:

$$\nabla\cdot\left(D_{\mathrm{p,O_2}}\nabla c_{\mathrm{p,O_2}}\right)-\frac{J_{\mathrm{e}}}{4F}=0 \tag{S12a}$$

$$\nabla\cdot\left(D_{\mathrm{p,H_2O}}\nabla c_{\mathrm{p,H_2O}}\right)-\frac{J_{\mathrm{e}}}{2F}\left(1+2n_d\right)=0 \tag{S12b}$$

$$\nabla\cdot\left(\sigma_{\mathrm{s}}\nabla\phi_{\mathrm{s}}\right)-J_{\mathrm{e}}=0 \tag{S12c}$$

$$\nabla\cdot\left(\kappa_{\mathrm{m}}\nabla\phi_{\mathrm{m}}\right)+J_{\mathrm{e}}=0 \tag{S12d}$$

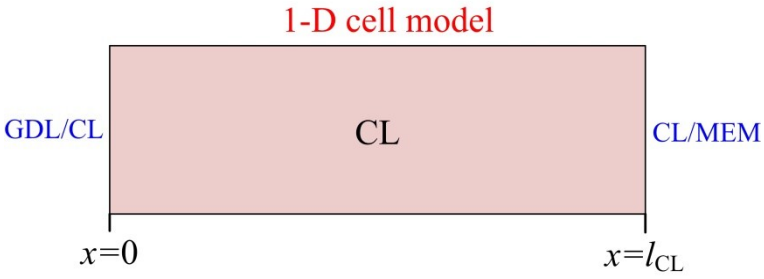

Fig. S4 Illustration of 1-D cathode CL model

The volumetric current density J_{e} is related to $R_{\mathrm{O_2}}^{\mathrm{Pt}}$ by

$$\frac{J_{\mathrm{e}}}{4F}=\left(\frac{f_{\mathrm{Pt}}}{l_{\mathrm{CL}}}\right)\frac{1}{R_{\mathrm{O_2}}^{\mathrm{Pt}}}\left(c_{\mathrm{p,O_2}}-c_{\mathrm{Pt,O_2}}\right) \tag{S13}$$

J_{e} is a product of the specific area of platinum a_{Pt} and the electrochemical reaction rate j. Boundary conditions for the oxygen and vapor transport at GDL/CL is related to the current density, which are the same with those mentioned in our paper (i.e., Eq. (28) at mesoscale level). They are described as follows,

$$\frac{c_{\mathrm{p,O_2}}\big|_{x=0}-c_{\mathrm{p,O_2}}^{\mathrm{in}}}{R_{\mathrm{O_2,CH+GDL}}}=\frac{i}{4F} \tag{S14a}$$

$$\frac{c_{\mathrm{p,H_2O}}\big|_{x=0}-c_{\mathrm{p,H_2O}}^{\mathrm{in}}}{R_{\mathrm{H_2O,CH+GDL}}}=-\frac{i}{2F}\left(1+2n_{\mathrm{d}}\right) \tag{S14b}$$

Boundary conditions for the charges are listed in Table S1. Consider the values σ_{s}=1000 s□m^{-1}, κ_{m}=1 s□m^{-1}, l_{CL}=12 μm, $D_{\mathrm{p,O2}}$=2.6×10^{-6} m^2□s^{-1}, $R_{\mathrm{O_2}}^{\mathrm{Pt}}$ =1282 s□m^{-1}, a_{ECSA}=57.4m^2□m^{-2}. The simulated cathode overpotential and protonic potential, together with the oxygen and water vapor concentration distribution, are illustrated in Fig. S5. It can be found that the protonic potential only changes 0.028V, and the cathode overpotential only varies 2.8% for

L_{Pt} = 0.40 mg□cm^{-2}. Therefore, the assumption of protonic isopotential condition adopted in the present study is reasonable for simulating the diffusion-limited transport processes of oxygen and vapor in CL.

Table S1 Boundary conditions for 1-D cathode model

Variable	GDL/CL	CL/PEM
ϕ_s	$\phi_s = 0.4$ V	$\nabla\phi_s = 0$
ϕ_m	$\nabla\phi_m = 0$	$\phi_m = 0$

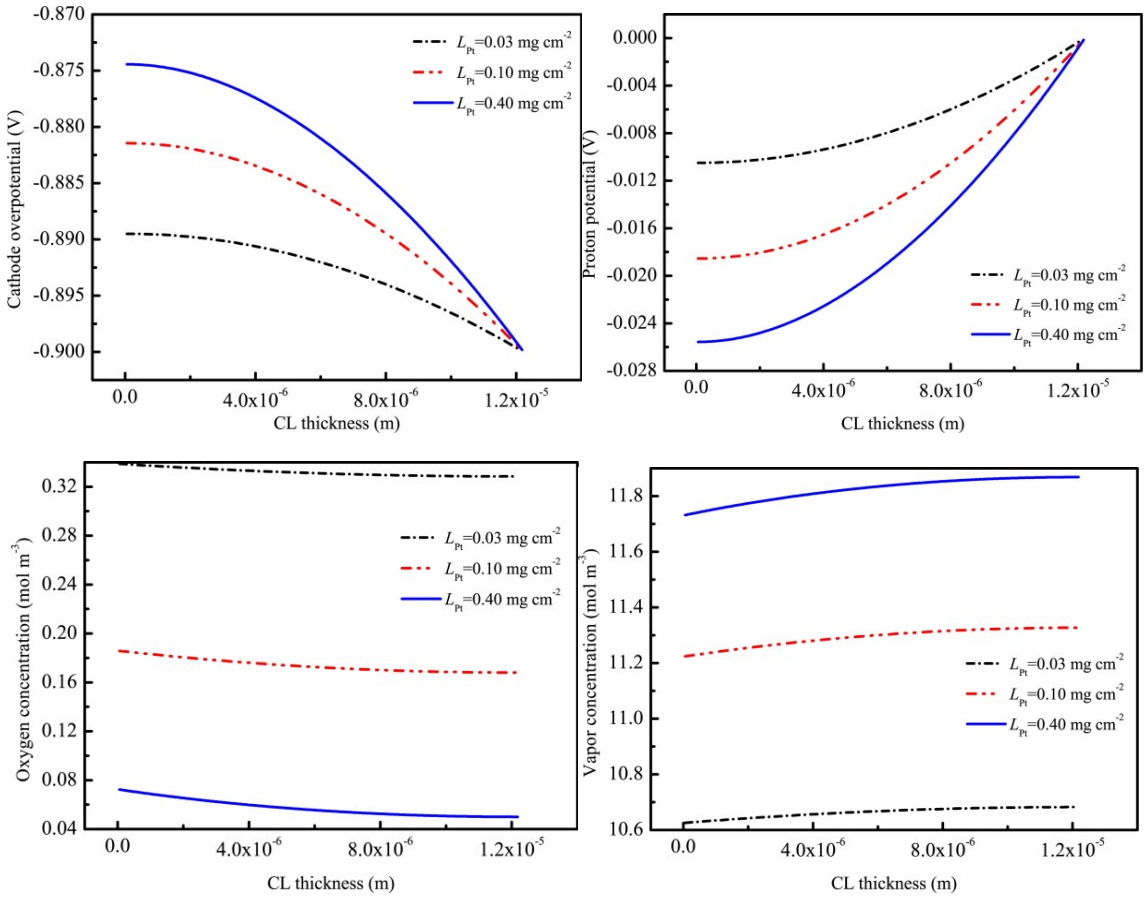

Fig. S5 Thickness-dependent key transport parameters

7. Ionomer thickness distributions for different γ

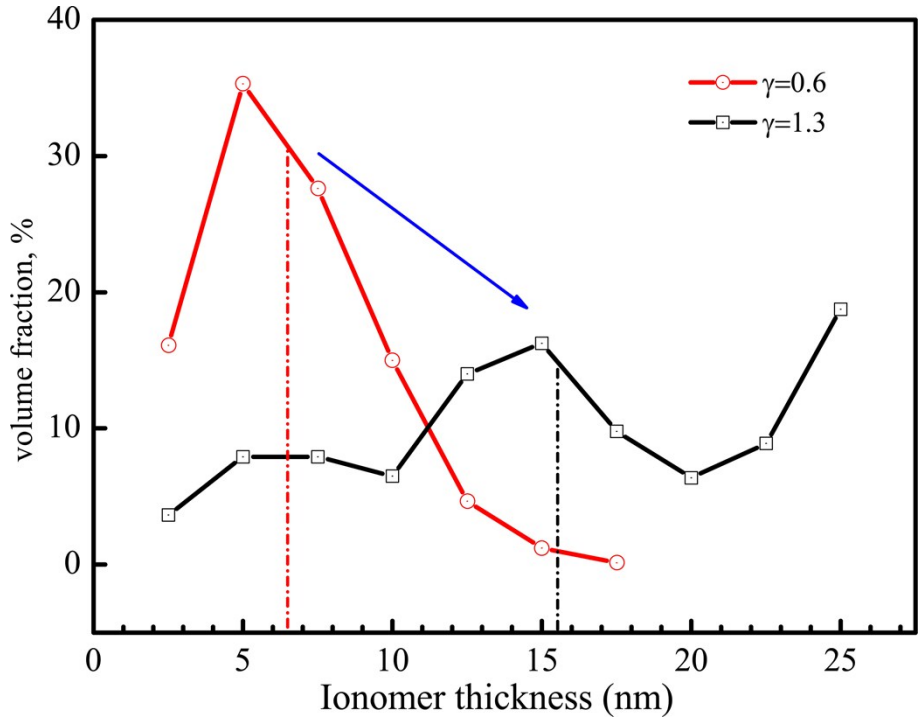

Fig. S6 Thicknesses of the ionomer thin-film versus γ

References

[1] Subramanian, N.P., T.A. Greszler, J. Zhang, W. Gu, and R. Makharia, *Pt-Oxide Coverage-Dependent Oxygen Reduction Reaction (ORR) Kinetics.* Journal of The Electrochemical Society, 2012. **159**(5): p. B531-B540.

[2] Hao, L., K. Moriyama, W. Gu, and C.-Y. Wang, *Modeling and Experimental Validation of Pt Loading and Electrode Composition Effects in PEM Fuel Cells.* Journal of The Electrochemical Society, 2015. **162**(8): p. F854-F867.

[3] Mu, Y.-T., P. He, J. Ding, and W.-Q. Tao, *Modeling of the operation conditions on the gas purging performance of polymer electrolyte membrane fuel cells.* International Journal of Hydrogen Energy, 2017. **42**(16): p. 11788-11802.

[4] Mu, Y.-T., L. Chen, Y.-L. He, Q.-J. Kang, and W.-Q. Tao, *Nucleate boiling performance evaluation of cavities at mesoscale level.* International Journal of Heat and Mass Transfer, 2017. **106**: p. 708-719.

[5] Mu, Y.-T., A.Z. Weber, Z.-L. Gu, and W.-Q. Tao, *Mesoscopic modeling of transport resistances in a polymer-electrolyte fuel-cell catalyst layer: Analysis of hydrogen limiting currents.* Applied Energy, 2019. **255**: p. 113895.

[6] Mu, Y.-T., Z.-L. Gu, P. He, and W.-Q. Tao, *Lattice Boltzmann method for conjugated heat and mass transfer with general interfacial conditions.* Physical Review E, 2018. **98**(4).